Compressed Semi-Discrete Central-Upwind Schemes for Hamilton-Jacobi Equations

Steve Bryson*, Alexander Kurganov†, Doron Levy‡ and Guergana Petrova§

Abstract

We introduce a new family of Godunov-type semi-discrete central schemes for multidimensional Hamilton-Jacobi equations. These schemes are a less dissipative generalization of the central-upwind schemes that have been recently proposed in series of works. We provide the details of the new family of methods in one, two, and three space dimensions, and then verify their expected low-dissipative property in a variety of examples.

AMS subject classification: Primary 65M06; Secondary 35L65

Key Words: Hamilton-Jacobi equations, central-upwind schemes, semi-discrete methods.

1 Introduction

We consider the multidimensional Hamilton-Jacobi equation,

$$\varphi_t + H(\nabla_{\mathbf{x}}\varphi) = 0, \quad \mathbf{x} \in \mathbb{R}^d, \tag{1.1}$$

with Hamiltonian H. First-order numerical schemes that converge to the viscosity solution of (1.1) were first introduced by Crandall and Lions in [5] and by Souganidis in [17]. Recent attempts to obtain higher-order approximate solutions of (1.1) include upwind methods, discontinuous Galerkin methods, and others. Here, we study a class of projection-evolution methods, called Godunov-type schemes. The main structure of these schemes is as follows: one starts with the point values of the solution, constructs an (essentially) non-oscillatory continuous piecewise polynomial interpolant, and then evolves it to the next time level while projecting the solution back onto the computational grid. The key idea in Godunov-type *central schemes* is to avoid solving (generalized) Riemann problems, by evolving (locally) smooth parts of the solution.

Second-order staggered Godunov-type central schemes were introduced by Lin and Tadmor in [14, 15]. L^1-convergence results for these schemes were obtained in [14]. More efficient non-staggered central schemes as well as genuinely multidimensional generalizations of the schemes in [15] were presented in [1], with high-order extensions (up to fifth-order) proposed in [2, 3].

*Program in Scientific Computing/Computational Mathematics, Stanford University and the NASA Advanced Supercomputing Division, NASA Ames Research Center, Moffett Field, CA 94035-1000; bryson@nas.nasa.gov

†Department of Mathematics, Tulane University, 6823 St. Charles Avenue, New Orleans, LA 70115; kurganov@math.tulane.edu, tel: +1-504-862-3443, fax: +1-504-865-5063

‡Department of Mathematics, Stanford University, Stanford, CA 94305-2125; dlevy@math.stanford.edu, tel: +1-650-723-4157, fax: +1-650-725-4066

§Department of Mathematics, Texas A&M University, College Station, TX 77843-3368; gpetrova@math.tamu.edu, tel: +1-979-845-5298, fax: +1-979-845-6028

Second-order semi-discrete Godunov-type central schemes were introduced in [12], where *local speeds* of propagation were employed to reduce the numerical dissipation. The numerical viscosity was further reduced in the *central-upwind* schemes [10] by utilizing one-sided estimates of the local speeds of propagation. Higher-order extensions of these schemes were introduced in [4], where weighted essentially non-oscillatory (WENO) interpolants were used to increase accuracy. WENO interpolants were originally developed for numerical methods for hyperbolic conservation laws [16, 8], and were first implemented in the context of upwind schemes for Hamilton-Jacobi equations in [7].

Godunov-type central-upwind schemes are constructed in two steps. First, the solution is evolved to the next time level on a nonuniform grid (the location of the grid points depends on the local speeds, and thus can vary at every time step). The solution is then projected back onto the original grid. The projection step requires an additional piecewise polynomial reconstruction over the nonuniform grid. In this paper we show that in the semi-discrete setting different choices of such a reconstruction lead to different numerical Hamiltonians, and thus to different schemes. In particular, we can recover the scheme from [10]. A more careful selection of the reconstruction results in a new central-upwind scheme with smaller numerical dissipation. This approach was originally proposed in [11], where it was applied to one-dimensional (1-D) systems of hyperbolic conservation laws. It has been recently generalized and implemented for multidimensional systems of hyperbolic conservation laws in [9].

The paper is organized as follows. In §2, we develop new semi-discrete central-upwind schemes for 1-D Hamilton-Jacobi equations. We also review the interpolants that are required to complete the construction of the second- and fifth-order schemes. Generalizations to more than one space dimensions (with special emphasis on the two-dimensional setup) are then presented in §3, where the corresponding multidimensional interpolants are also discussed. In §4, we evaluate the performance of the new schemes with a series of numerical tests. Finally, in the Appendix, we prove the monotonicity of the new numerical Hamiltonian.

2 One-Dimensional Schemes

2.1 Semi-Discrete Central-Upwind Schemes for Hamilton-Jacobi Equations

In this section, we describe the derivation of a new family of semi-discrete central-upwind schemes for the 1-D Hamilton-Jacobi equation,

$$\varphi_t + H(\varphi_x) = 0, \qquad x \in \mathbb{R}, \tag{2.1}$$

subject to the initial data $\varphi(x, t = 0) = \varphi_0(x)$. We follow the approach in [10] (see also [12]). For simplicity we assume a uniform grid in space and time with grid spacing Δx and Δt, respectively. The grid points are denoted by $x_j := j\Delta x$, $t^n := n\Delta t$, and the approximate value of $\varphi(x_j, t^n)$ is denoted by φ_j^n.

Assume that the approximate solution at time t^n, φ_j^n, is given, and that a continuous piecewise-polynomial interpolant $\widetilde{\varphi}(x, t^n)$ is reconstructed from φ_j^n. At every grid point, the maximal right and left speeds of propagation, a_j^+ and a_j^-, are then estimated by

$$a_j^+ = \max_{\min\{\varphi_x^-, \varphi_x^+\} \le u \le \max\{\varphi_x^-, \varphi_x^+\}} \left\{H'(u), 0\right\}, \quad a_j^- = \left| \min_{\min\{\varphi_x^-, \varphi_x^+\} \le u \le \max\{\varphi_x^-, \varphi_x^+\}} \left\{H'(u), 0\right\} \right|, \tag{2.2}$$

where $\varphi_x^\pm$ are the one-sided derivatives at $x = x_j$, that is

$$\varphi_x^\pm := \widetilde{\varphi}_x(x_j \pm 0, t^n).$$

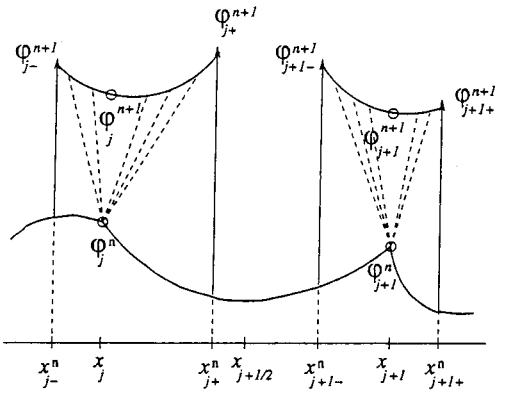

Figure 2.1: Central-upwind differencing: 1-D

If the Hamiltonian is convex, (2.2) reduces to

$$a_j^+ = \max\left\{H'(\varphi_x^-), H'(\varphi_x^+), 0\right\}, \quad a_j^- = \left|\min\left\{H'(\varphi_x^-), H'(\varphi_x^+), 0\right\}\right|. \tag{2.3}$$

We then proceed by evolving the reconstruction $\widetilde{\varphi}$ at the evolution points $x_{j\pm}^n := x_j \pm a_j^{\pm}\Delta t$, to the next time level according to (2.1). The time step Δt is chosen so that $x_{j+}^n < x_{(j+1)-}^n$ for all j. Therefore the solution remains smooth at $x_{j\pm}^n$ for $t \in [t^n, t^{n+1}]$ (see Figure 2.1) and we can compute the values of the evolved solution $\{\varphi_{j\pm}^{n+1}\}$ by the Taylor expansion:

$$\varphi_{j\pm}^{n+1} = \widetilde{\varphi}(x_{j\pm}^n, t^n) - \Delta t H\left(\widetilde{\varphi}_x(x_{j\pm}^n, t^n)\right) + O\left(\Delta t^2\right). \tag{2.4}$$

Using the values $\{\varphi_{j\pm}^{n+1}\}$ on the nonuniform grid $\{x_{j\pm}^n\}$, we construct a new quadratic interpolant $\widetilde{\psi}(x, t^{n+1})$ on the interval $[x_{j-}^n, x_{j+}^n]$,

$$\widetilde{\psi}\left(x, t^{n+1}\right) := \varphi_{j-}^{n+1} + \frac{\varphi_{j+}^{n+1} - \varphi_{j-}^{n+1}}{x_{j+}^n - x_{j-}^n}\left(x - x_{j-}^n\right) + \frac{1}{2}(\widehat{\varphi}_{xx})_j^{n+1}(x - x_{j-}^n)(x - x_{j+}^n), \tag{2.5}$$

where $(\widehat{\varphi}_{xx})_j^{n+1}$ is yet to be determined and is an approximation to $\varphi_{xx}(\widehat{x}_j^n, t^{n+1})$, $\widehat{x}_j^n = (x_{j+}^n + x_{j-}^n)/2$. The projection back onto the original grid is then carried out by evaluating $\widetilde{\psi}(x, t^{n+1})$ at x_j,

$$\varphi_j^{n+1} := \widetilde{\psi}(x_j, t^{n+1}) = \frac{a_j^+}{a_j^+ + a_j^-}\varphi_{j-}^{n+1} + \frac{a_j^-}{a_j^+ + a_j^-}\varphi_{j+}^{n+1} - \frac{1}{2}(\widehat{\varphi}_{xx})_j^{n+1} a_j^+ a_j^- (\Delta t)^2. \tag{2.6}$$

Note that if the Riemann fan is symmetric, that is, if $a_j^+ = a_j^-$, then $\widehat{x}_j^n = x_j$. Substituting (2.4) in (2.6) yields

$$\begin{aligned}\varphi_j^{n+1} = {} & \frac{a_j^+}{a_j^+ + a_j^-}\Big(\widetilde{\varphi}(x_{j-}^n, t^n) - \Delta t H(\widetilde{\varphi}_x(x_{j-}^n, t^n))\Big) \\ & + \frac{a_j^-}{a_j^+ + a_j^-}\Big(\widetilde{\varphi}(x_{j+}^n, t^n) - \Delta t H(\widetilde{\varphi}_x(x_{j+}^n, t^n))\Big) - \frac{1}{2}(\widehat{\varphi}_{xx})_j^{n+1} a_j^+ a_j^- (\Delta t)^2 + \mathcal{O}(\Delta t)^2.\end{aligned} \tag{2.7}$$

Using the Taylor expansion,

$$\widetilde{\varphi}(x_{j\pm}^n, t^n) = \varphi_j^n \pm \Delta t a_j^{\pm}\varphi_x^{\pm} + \mathcal{O}(\Delta t)^2, \tag{2.8}$$

we arrive at

$$\varphi_j^{n+1} = \varphi_j^n + \Delta t \frac{a_j^+ a_j^-}{a_j^+ + a_j^-}\left(\varphi_x^+ - \varphi_x^-\right) - \frac{\Delta t}{a_j^+ + a_j^-}\left[a_j^- H(\widetilde{\varphi}_x(x_{j+}^n, t^n)) + a_j^+ H(\widetilde{\varphi}_x(x_{j-}^n, t^n))\right]$$
$$-\frac{1}{2}(\widehat{\varphi}_{xx})_j^{n+1} a_j^+ a_j^- (\Delta t)^2 + \mathcal{O}(\Delta t)^2. \tag{2.9}$$

We then let $\Delta t \to 0$, and end up with the (family of) semi-discrete central-upwind schemes:

$$\frac{d}{dt}\varphi_j(t) = -\frac{a_j^- H(\varphi_x^+) + a_j^+ H(\varphi_x^-)}{a_j^+ + a_j^-} + a_j^+ a_j^-\left(\frac{\varphi_x^+ - \varphi_x^-}{a_j^+ + a_j^-} - \frac{1}{2}\lim_{\Delta t\to 0}\left[\Delta t(\widehat{\varphi}_{xx})_j^{n+1}\right]\right). \tag{2.10}$$

Here, the one-sided speeds of propagation, $a_j^\pm$, are given by (2.2), and $\varphi_x^\pm$ are the left and right derivatives at the point $x = x_j$ of the reconstruction $\widetilde{\varphi}(\cdot, t)$ at time t.

Finally, in order to complete the construction of the scheme, we must determine $(\widehat{\varphi}_{xx})_j^{n+1}$. For example, selecting $(\widehat{\varphi}_{xx})_j^{n+1}$ to be independent of Δt gives

$$\lim_{\Delta t\to 0}\left[\Delta t(\widehat{\varphi}_{xx})_j^{n+1}\right] = 0,$$

and then (2.10) recovers the central-upwind scheme in [10]. However, since the interpolant $\widetilde{\psi}(\cdot, t^{n+1})$ is defined on the intervals $[x_{j-}^n, x_{j+}^n]$, whose size is proportional to Δt, it is natural to choose $(\widehat{\varphi}_{xx})_j^{n+1}$ to be proportional to $1/\Delta t$. In this case, the approximation of the second derivative in (2.10) will add a non-zero contribution to the limit as $\Delta t \to 0$. At the same time, to guarantee a non-oscillatory reconstruction, we should use a nonlinear limiter. For example, one can use the minmod limiter:

$$\Delta t(\widehat{\varphi}_{xx})_j^{n+1} = 2\text{minmod}\left(\frac{\widetilde{\varphi}_x(x_{j+}^n, t^{n+1}) - \widetilde{\psi}_x(\widehat{x}_j^n, t^{n+1})}{a_j^+ + a_j^-}, \frac{\widetilde{\psi}_x(\widehat{x}_j^n, t^{n+1}) - \widetilde{\varphi}_x(x_{j-}^n, t^{n+1})}{a_j^+ + a_j^-}\right), \tag{2.11}$$

where $\widetilde{\psi}_x$ is the derivative of (2.5), $\widetilde{\varphi}_x(x_{j\pm}^n, t^{n+1})$ are the values of the derivative of the evolved reconstruction $\widetilde{\varphi}(\cdot, t^n)$ at $t = t^{n+1}$, and the multivariate minmod function is defined by

$$\text{minmod}(x_1, x_2, ...) := \begin{cases} \min\limits_j\{x_j\}, & \text{if } x_j > 0 \ \ \forall j, \\ \max\limits_j\{x_j\}, & \text{if } x_j < 0 \ \ \forall j, \\ 0, & \text{otherwise.} \end{cases} \tag{2.12}$$

A different choice of limiter will result in a different scheme from the same family of central-upwind schemes.

All that remains is to determine the quantities used in (2.11). Since all data are smooth along the line segments $(x_{j\pm}^n, t)$, $t^n \le t < t^{n+1}$, we can use a Taylor expansion to obtain

$$\widetilde{\varphi}_x(x_{j\pm}^n, t^{n+1}) = \widetilde{\varphi}_x(x_{j\pm}^n, t^n) + O(\Delta t). \tag{2.13}$$

According to (2.5), the derivative $\widetilde{\psi}_x(\widehat{x}_j^n, t^{n+1})$ of the new reconstruction $\widetilde{\psi}$ at time level t^{n+1} is

$$\widetilde{\psi}_x(\widehat{x}_j^n, t^{n+1}) = \frac{\varphi_{j+}^{n+1} - \varphi_{j-}^{n+1}}{(a_j^+ + a_j^-)\Delta t}, \tag{2.14}$$

and after substituting (2.4) and (2.8) into (2.14), we obtain

$$\widetilde{\psi}_x(\widehat{x}_j^n, t^{n+1}) = \frac{a_j^+\varphi_x^+ + a_j^-\varphi_x^-}{(a_j^+ + a_j^-)} - \frac{H(\widetilde{\varphi}_x(x_{j+}^n, t^n)) - H(\widetilde{\varphi}_x(x_{j-}^n, t^n))}{(a_j^+ + a_j^-)} + \mathcal{O}(\Delta t). \tag{2.15}$$

Passing to the semi-discrete limit ($\Delta t \to 0$) in (2.11), (2.13), and (2.15) gives

$$\lim_{\Delta t\to 0}\left[\Delta t(\widehat{\varphi}_{xx})_j^{n+1}\right]=\frac{2}{(a_j^+ + a_j^-)}\,\text{minmod}\left(\varphi_x^+ - \psi_x^{\text{int}}, \psi_x^{\text{int}} - \varphi_x^-\right), \tag{2.16}$$

where

$$\psi_x^{\text{int}} := \lim_{\Delta t\to 0}[\widetilde{\psi}_x(\widehat{x}_j^n, t^{n+1})] = \frac{a_j^+\varphi_x^+ + a_j^-\varphi_x^-}{(a_j^+ + a_j^-)} - \frac{H(\varphi_x^+) - H(\varphi_x^-)}{(a_j^+ + a_j^-)}. \tag{2.17}$$

Finally, substituting (2.16) into (2.10), we obtain the 1-D *low-dissipative semi-discrete central-upwind scheme*:

$$\frac{d}{dt}\varphi_j(t) = -\frac{a_j^- H(\varphi_x^+) + a_j^+ H(\varphi_x^-)}{a_j^+ + a_j^-} + a_j^+ a_j^-\left[\frac{\varphi_x^+ - \varphi_x^-}{a_j^+ + a_j^-} - \text{minmod}\left(\frac{\varphi_x^+ - \psi_x^{\text{int}}}{a_j^+ + a_j^-}, \frac{\psi_x^{\text{int}} - \varphi_x^-}{a_j^+ + a_j^-}\right)\right], \tag{2.18}$$

where ψ_x^{int} is given by (2.17). For future reference, we denote the RHS of (2.18) by $-H^{BKLP}$.

Notice, that in the fully-discrete setting the use of the intermediate quadratic reconstruction $\widetilde{\psi}(\cdot, t^{n+1})$ at level t^{n+1} (as opposed to the intermediate piecewise linear reconstruction in [10]) increases the accuracy of the resulting fully-discrete scheme: $\mathcal{O}((\Delta t)^2 + (\Delta x)^r)$ versus $\mathcal{O}(\Delta t + (\Delta x)^r)$, where r is the (formal) order of accuracy of the continuous piecewise polynomial reconstruction $\widetilde{\varphi}(\cdot, t^n)$. When we pass to the semi-discrete limit ($\Delta t \to 0$), both quadratic and linear interpolation errors go to 0, and therefore the (formal) order of accuracy of both (2.17)–(2.18) and the semi-discrete scheme in [10] is $\mathcal{O}((\Delta x)^r)$, and the temporal error is determined solely by the (formal) order of accuracy of the ODE solver used to integrate (2.18). However, the minmod limiter introduces a new term that leads to a reduction of the numerical dissipation without affecting the accuracy of the scheme. To demonstrate this, we show that ψ_x^{int} is always in the interval $[\min\{\varphi_x^+, \varphi_x^-\}, \max\{\varphi_x^+, \varphi_x^-\}]$, and therefore the absolute value of the term $(\varphi_x^+ - \varphi_x^-)$ in the numerical dissipation in the scheme from [10] is always greater than the absolute value of the new term, that is

$$\left|\varphi_x^+ - \varphi_x^-\right| \geq \left|\varphi_x^+ - \varphi_x^- - \text{minmod}\left(\varphi_x^+ - \psi_x^{\text{int}}, \psi_x^{\text{int}} - \varphi_x^-\right)\right|.$$

Indeed, we have

$$\psi_x^{\text{int}} = \frac{a_j^+\varphi_x^+ + a_j^-\varphi_x^-}{(a_j^+ + a_j^-)} - \frac{H(\varphi_x^+) - H(\varphi_x^-)}{(a_j^+ + a_j^-)} = \varphi_x^+\left[\frac{a_j^+ - H'(\xi)}{a_j^+ + a_j^-}\right] + \varphi_x^-\left[\frac{H'(\xi) + a_j^-}{a_j^+ + a_j^-}\right], \tag{2.19}$$

where $\xi \in (\min\{\varphi_x^+, \varphi_x^-\}, \max\{\varphi_x^+, \varphi_x^-\})$. It follows from the definition of the local speeds (2.2) that

$$a_j^+ - H'(\xi) \geq 0, \quad H'(\xi) + a_j^- \geq 0.$$

Thus, (2.19) is a convex combination of φ_x^+ and φ_x^-, and therefore $\psi_x^{\text{int}} \in [\min\{\varphi_x^+, \varphi_x^-\}, \max\{\varphi_x^+, \varphi_x^-\}]$

It was shown in [4] that the numerical Hamiltonian H^{KNP} from [10] is monotone, provided that the Hamiltonian H is convex. Here, we state a theorem about the monotonicity of H^{BKLP} — the new, less dissipative Hamiltonian in (2.18). The proof is left to the Appendix. We will consider only Hamiltonians for which H' changes sign, because otherwise either $a^- \equiv 0$ or $a^+ \equiv 0$ and the Hamiltonian in (2.18) reduces to the upwind one for which such a theorem is known.

Theorem 2.1 *Let the Hamiltonian $H \in C^2$ be convex and satisfy the following two assumptions:*

(A1) The function

$$G(u,v) := 2H''(u)\left[(u-v)H'(v) - (H(u) - H(v))\right] + \left[H'(u) - H'(v)\right]^2 \leq 0 \tag{2.20}$$

for all u and v in the set $S^-(u,v) \cup S^+(u,v)$, where

$$S^-(u,v) := \left\{(u,v) : \frac{H(u)-H(v)}{u-v} \le \frac{H'(u)+H'(v)}{2},\ u \ge u^* \ge v\right\},$$
$$S^+(u,v) := \left\{(u,v) : \frac{H(u)-H(v)}{u-v} \ge \frac{H'(u)+H'(v)}{2},\ u \le u^* \le v\right\}, \tag{2.21}$$

and u^* is the only point such that $H'(u^*)=0$;

(A2) For any v and for an arbitrary interval $[a,b]$, the sets $S^-(u,v)\cap[a,b]$ and $S^+(u,v)\cap[a,b]$ are either the empty set or finite unions of closed intervals and/or points.

Then the numerical Hamiltonian in (2.18)*:*

$$\begin{aligned} H^{BKLP}(u^+,u^-) &:= \frac{a^-H(u^+)+a^+H(u^-)}{a^++a^-} \\ &- a^+a^-\left[\frac{u^+-u^-}{a^++a^-} - \text{minmod}\left(\frac{u^+-u^{\text{int}}}{a^++a^-}, \frac{u^{\text{int}}-u^-}{a^++a^-}\right)\right], \end{aligned} \tag{2.22}$$

where

$$u^{\text{int}} := \frac{a^+u^+ + a^-u^-}{(a^++a^-)} - \frac{H(u^+)-H(u^-)}{(a^++a^-)},$$

and $a^+ := a^+(u^+,u^-) = \max\{H'(u^+),H'(u^-),0\}$, $a^- := a^-(u^+,u^-) = |\min\{H'(u^+),H'(u^-),0\}|$ is monotone, that is, H^{BKLP} is a non-increasing function of u^+ and a non-decreasing function of u^-.

Remarks.
1. The classification of all Hamiltonians that satisfy conditions (2.20)–(2.21) is an open problem. However, we were able to verify these conditions for certain Hamiltonians. For example, a straightforward computation shows that for any convex quadratic Hamiltonians $H(u)=au^2+bu+c$, the function $G(u,v)\equiv 0$, the sets in *(A2)* are either $\varnothing$ or one closed interval, or one point, and therefore the theorem holds.
Another example, for which Theorem 2.1 is valid, is $H(u)=u^4$. In this case, the sets (2.21) are

$$S^-(u,v) = \{(u,v) : u+v \ge 0 \ge v\}, \quad S^+(u,v) = \{(u,v) : u+v \le 0 \le v\},$$

and, as one can easily verify, the function

$$G(u,v) = -8(u-v)^3(u^3+3u^2v+6uv^2+2v^3) \le 0,$$

in $S^-(u,v)\cup S^+(u,v)$. As for the sets in assumption *(A2)*, they are either $\varnothing$ or one closed interval, or one point.
2. Notice that assumption *(A2)* in Theorem 2.1 is needed only for technical purposes and in fact it is satisfied by (almost) every Hamiltonian H that arises in applications.

2.2 A Second-Order Scheme

A non-oscillatory second-order scheme can be obtained if one uses a non-oscillatory continuous piecewise quadratic interpolant $\widetilde{\varphi}$. The values of the one-sided derivatives of $\widetilde{\varphi}$ at (x_j,t^n) in (2.17) and (2.18), are given by

$$\varphi_x^{\pm} = \frac{(\Delta\varphi)^n_{j\pm\frac12}}{\Delta x} \mp \frac{\Delta x}{2}(\varphi_{xx})^n_{j+\frac12}, \qquad (\Delta\varphi)^n_{j+\frac12} := \varphi^n_{j+1}-\varphi^n_j, \tag{2.23}$$

where the second derivative is computed with a nonlinear limiter. For example,

$$(\varphi_{xx})^n_{j+\frac{1}{2}} = \text{minmod}\left(\theta\frac{(\Delta\varphi)^n_{j+\frac{3}{2}} - (\Delta\varphi)^n_{j+\frac{1}{2}}}{(\Delta x)^2}, \frac{(\Delta\varphi)^n_{j+\frac{3}{2}} - (\Delta\varphi)^n_{j-\frac{1}{2}}}{2(\Delta x)^2}, \theta\frac{(\Delta\varphi)^n_{j+\frac{1}{2}} - (\Delta\varphi)^n_{j-\frac{1}{2}}}{(\Delta x)^2}\right). \quad (2.24)$$

Here, $\theta \in [1,2]$ and the minmod function is given by (2.12). The scheme requires a second-order ODE solver.

2.3 Higher-Order Schemes

In this section, we briefly describe the third- and fifth-order weighted essentially non-oscillatory (WENO) reconstructions. They were derived in [4] in the context of central-upwind schemes, and are similar to those used in high-order upwind schemes [7].

In smooth regions, the WENO reconstructions use a convex combination of multiple overlapping reconstructions to attain high order accuracy. In nonsmooth regions, a smoothness measure is employed to increase the weight of the least oscillatory reconstruction. Here, we reconstruct the one-sided derivatives $(\varphi^{\pm}_x)_{k,j}$ at $x = x_j$ for $k = 1,\dots,d$ stencils, and write the convex combination:

$$\varphi^{\pm}_x = \sum_{k=1}^{d} w^{\pm}_{k,j}(\varphi^{\pm}_x)_{k,j}, \qquad \sum_{k=1}^{d} w^{\pm}_{k,j} = 1, \qquad w^{\pm}_{k,j} \geq 0, \quad (2.25)$$

where the values $\varphi^{\pm}_x$ are to be used in the scheme (2.17)–(2.18). The weights $w^{\pm}_{k,j}$ are defined as

$$w^{\pm}_{k,j} = \frac{\alpha^{\pm}_{k,j}}{\sum\limits_{l=1}^{d}\alpha^{\pm}_{l,j}}, \qquad \alpha^{\pm}_{k,j} = \frac{c^{\pm}_k}{\left(\epsilon + S^{\pm}_{k,j}\right)^p}. \quad (2.26)$$

The constants $c^{\pm}_k$ are set so that the convex combination in (2.25) is of the maximal possible order of accuracy in smooth regions. We take $p = 2$ and choose $\epsilon = 10^{-6}$ to prevent the denominator in (2.26) from vanishing.

A third-order WENO reconstruction is obtained in the case $d = 2$ with

$$(\varphi^{+}_x)_{1,j} = \frac{\varphi_{j+1} - \varphi_{j-1}}{2\Delta x}, \qquad (\varphi^{-}_x)_{1,j} = \frac{-\varphi_{j-2} + 4\varphi_{j-1} - 3\varphi_j}{2\Delta x},$$
$$(\varphi^{+}_x)_{2,j} = \frac{-3\varphi_j + 4\varphi_{j+1} - \varphi_{j+2}}{2\Delta x}, \qquad (\varphi^{-}_x)_{2,j} = \frac{\varphi_{j+1} - \varphi_{j-1}}{2\Delta x}.$$

The constants $c^{\pm}_k$ are given by

$$c^{+}_1 = c^{-}_2 = \frac{2}{3}, \quad c^{+}_2 = c^{-}_1 = \frac{1}{3},$$

and the smoothness measures are

$$S^{+}_{1,j} = S_j[-1,0], \quad S^{+}_{2,j} = S_j[0,1], \quad S^{-}_{1,j} = S_j[-2,-1], \quad S^{-}_{2,j} = S_j[-1,0].$$

Here,

$$S_j[r,s] := \Delta x\sum_{i=r}^{s}\left(\frac{\Delta^+\varphi_{j+i}}{\Delta x}\right)^2 + \Delta x\sum_{i=r+1}^{s}\left(\frac{\Delta^+\Delta^-\varphi_{j+i}}{\Delta x^2}\right)^2, \quad \Delta^{\pm}\varphi_j := \pm(\varphi_{j\pm1} - \varphi_j). \quad (2.27)$$

A fifth-order WENO reconstruction is obtained when $d = 3$. In this case,

$$(\varphi_x^+)_{1,j} = \frac{\varphi_{j-2} - 6\varphi_{j-1} + 3\varphi_j + 2\varphi_{j+1}}{6\Delta x}, \qquad (\varphi_x^-)_{1,j} = \frac{2\varphi_{j-3} - 9\varphi_{j-2} + 18\varphi_{j-1} - 11\varphi_j}{6\Delta x},$$
$$(\varphi_x^+)_{2,j} = \frac{-2\varphi_{j-1} - 3\varphi_j + 6\varphi_{j+1} - \varphi_{j+2}}{6\Delta x}, \qquad (\varphi_x^-)_{2,j} = \frac{-\varphi_{j-2} + 6\varphi_{j-1} - 3\varphi_j - 2\varphi_{j+1}}{6\Delta x},$$
$$(\varphi_x^+)_{3,j} = \frac{-11\varphi_j + 18\varphi_{j+1} - 9\varphi_{j+2} + 2\varphi_{j+3}}{6\Delta x}, \qquad (\varphi_x^-)_{3,j} = \frac{2\varphi_{j-1} + 3\varphi_j - 6\varphi_{j+1} + \varphi_{j+2}}{6\Delta x}.$$

The constants $c_k^{\pm}$ are given by

$$c_1^+ = c_3^- = \frac{3}{10}, \quad c_3^+ = c_1^- = \frac{1}{10}, \quad c_2^{\pm} = \frac{3}{5},$$

and the smoothness measures are

$$S_{1,j}^+ = S_j\,[-2,0]\,, \quad S_{2,j}^+ = S_j\,[-1,1]\,, \quad S_{3,j}^+ = S_j\,[0,2]\,,$$
$$S_{1,j}^- = S_j\,[-3,-1]\,, \quad S_{2,j}^- = S_j\,[-2,0]\,, \quad S_{3,j}^- = S_j\,[-1,1]\,.$$

The time evolution of (2.18) should be performed with an ODE solver whose order of accuracy is compatible with the spatial order of the scheme. In our numerical examples, we use the strong stability preserving (SSP) Runge-Kutta methods from [6].

3 Multidimensional Schemes

In this section, we derive the two-dimensional (2-D) generalization of the compressed semi-discrete central-upwind scheme (2.17)–(2.18), and then extend it to three space dimensions. We also comment on the multidimensional interpolants that these extensions require.

3.1 A Two-Dimensional Scheme

We consider the 2-D Hamilton-Jacobi equation,

$$\varphi_t + H(\varphi_x, \varphi_y) = 0, \tag{3.1}$$

and proceed as in [10]. We assume that at time $t = t^n$ the approximate point values $\varphi_{jk}^n \approx \varphi(x_j, y_k, t^n)$ are given, and construct a 2-D continuous piecewise-quadratic interpolant, $\widetilde{\varphi}(x, y, t^n)$, defined on the cells $S_{jk} := \{(x,y) : \frac{|x-x_j|}{\Delta x} + \frac{|y-y_k|}{\Delta y} \le 1\}$. On each cell S_{jk} there will be four such interpolants (labeled NW, NE, SE, and SW), one for each triangle that constitutes S_{jk} (see Figure 3.1). Specific examples of $\widetilde{\varphi}(x, y, t^n)$ are discussed in §3.3.

Similarly to the 1-D case, we use the maximal values of the one-sided local speeds of propagation in the x- and y-directions to estimate the widths of the local Riemann fans. These values at any grid point (x_j, y_k) are given by

$$a_{jk}^+ := \max_{C_{jk}} \Big\{ H_u(\widetilde{\varphi}_x(x,y,t), \widetilde{\varphi}_y(x,y,t)) \Big\}_+, \quad a_{jk}^- := \Big| \min_{C_{jk}} \Big\{ H_u(\widetilde{\varphi}_x(x,y,t), \widetilde{\varphi}_y(x,y,t)) \Big\}_- \Big|,$$
$$b_{jk}^+ := \max_{C_{jk}} \Big\{ H_v(\widetilde{\varphi}_x(x,y,t), \widetilde{\varphi}_y(x,y,t)) \Big\}_+, \quad b_{jk}^- := \Big| \min_{C_{jk}} \Big\{ H_v(\widetilde{\varphi}_x(x,y,t), \widetilde{\varphi}_y(x,y,t)) \Big\}_- \Big|, \tag{3.2}$$

where $C_{jk} := [x_{j-\frac{1}{2}}, x_{j+\frac{1}{2}}] \times [y_{k-\frac{1}{2}}, y_{k+\frac{1}{2}}]$, $(\cdot)_+ := \max(\cdot, 0)$, $(\cdot)_- := \min(\cdot, 0)$, and $(H_u, H_v)^T$ is the gradient of H.

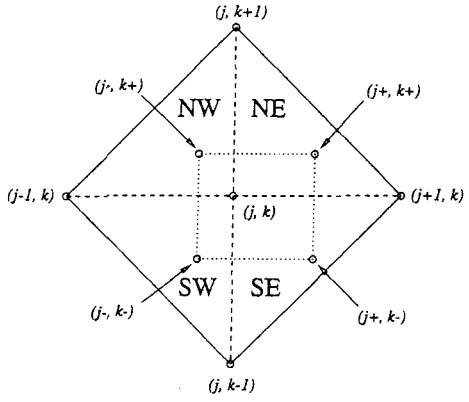

Figure 3.1: Central-upwind differencing: 2-D

The reconstruction $\widetilde{\varphi}(x,y,t^n)$ is then evolved according to the Hamilton-Jacobi equation (3.1). Due to the finite speed of propagation, for sufficiently small Δt, the solution of (3.1) with initial data $\widetilde{\varphi}$ is smooth around $(x^n_{j\pm}, y^n_{k\pm})$ where $x^n_{j\pm} := x_j \pm a^{\pm}_{jk}\Delta t$, $y^n_{k\pm} := y_k \pm b^{\pm}_{jk}\Delta t$, see Figure 3.1. We denote by $\widetilde{\varphi}^n_{j\pm,k\pm} := \widetilde{\varphi}(x^n_{j\pm}, y^n_{k\pm}, t^n)$, and use the Taylor expansion to calculate the intermediate values at the next time level $t = t^{n+1}$

$$\varphi^{n+1}_{j\pm,k\pm} = \widetilde{\varphi}^n_{j\pm,k\pm} - \Delta t \cdot H(\widetilde{\varphi}_x(x^n_{j\pm}, y^n_{k\pm}, t^n), \widetilde{\varphi}_y(x^n_{j\pm}, y^n_{k\pm}, t^n)) + \mathcal{O}(\Delta t)^2. \tag{3.3}$$

We now project the intermediate values $\varphi^{n+1}_{j\pm,k\pm}$ onto the original grid points (x_j, y_k). First, similarly to (2.5), we use new 1-D quadratic interpolants in the y-direction, $\widetilde{\psi}(x^n_{j\pm}, \cdot, t^{n+1})$, to obtain

$$\begin{aligned}\widetilde{\psi}(x^n_{j\pm}, y_k, t^{n+1}) &= \varphi^{n+1}_{j\pm,k-} + \frac{\varphi^{n+1}_{j\pm,k+} - \varphi^{n+1}_{j\pm,k-}}{b^+_{jk} + b^-_{jk}} b^-_{jk} - \frac{1}{2}(\widehat{\varphi}_{yy})^{n+1}_{j\pm,k} b^+_{jk} b^-_{jk} (\Delta t)^2 \\ &= \frac{b^+_{jk}}{b^+_{jk} + b^-_{jk}} \varphi^{n+1}_{j\pm,k-} + \frac{b^-_{jk}}{b^+_{jk} + b^-_{jk}} \varphi^{n+1}_{j\pm,k+} - \frac{1}{2}(\widehat{\varphi}_{yy})^{n+1}_{j\pm,k} b^+_{jk} b^-_{jk} (\Delta t)^2,\end{aligned} \tag{3.4}$$

where $(\widehat{\varphi}_{yy})^{n+1}_{j\pm,k} \approx \varphi_{yy}(x^n_{j\pm}, \widehat{y}^n_k, t^{n+1})$ and $\widehat{y}^n_k := (y^n_{k+} + y^n_{k-})/2$. Next, we use the values $\widetilde{\psi}(x^n_{j\pm}, y_k, t^{n+1})$ to construct another 1-D quadratic interpolant $\widetilde{\phi}(\cdot, y_k, t^{n+1})$, this time in the x-direction, whose values at the original grid points are

$$\begin{aligned}\varphi^{n+1}_{jk} &:= \widetilde{\phi}(x_j, y_k, t^{n+1}) \\ &= \frac{a^+_{jk}}{a^+_{jk} + a^-_{jk}} \widetilde{\psi}(x^n_{j-}, y_k, t^{n+1}) + \frac{a^-_{jk}}{a^+_{jk} + a^-_{jk}} \widetilde{\psi}(x^n_{j+}, y_k, t^{n+1}) - \frac{1}{2}(\widehat{\varphi}_{xx})^{n+1}_{j,k} a^+_{jk} a^-_{jk} (\Delta t)^2.\end{aligned} \tag{3.5}$$

Here, $(\widehat{\varphi}_{xx})^{n+1}_{j,k} \approx \varphi_{xx}(\widehat{x}^n_j, y_k, t^{n+1})$ and $\widehat{x}^n_j := (x^n_{j+} + x^n_{j-})/2$. We choose $(\widehat{\varphi}_{xx})^{n+1}_{j,k}$ to be the weighted average

$$(\widehat{\varphi}_{xx})^{n+1}_{j,k} = \frac{b^+_{jk}}{b^+_{jk} + b^-_{jk}} (\widehat{\varphi}_{xx})^{n+1}_{j,k-} + \frac{b^-_{jk}}{b^+_{jk} + b^-_{jk}} (\widehat{\varphi}_{xx})^{n+1}_{j,k+}, \qquad (\widehat{\varphi}_{xx})^{n+1}_{j,k\pm} \approx \varphi_{xx}(\widehat{x}^n_j, y^n_{k\pm}, t^{n+1}). \tag{3.6}$$

Notice that both $(\widehat{\varphi}_{yy})^{n+1}_{j\pm,k}$ in (3.4) and $(\widehat{\varphi}_{xx})^{n+1}_{j,k\pm}$ in (3.6) are yet to be determined.

We then substitute (3.4) and (3.6) into (3.5), and obtain

$$\begin{aligned}\varphi_{jk}^{n+1} &= \frac{a_{jk}^- b_{jk}^- \varphi_{j+,k+}^{n+1} + a_{jk}^- b_{jk}^+ \varphi_{j+,k-}^{n+1} + a_{jk}^+ b_{jk}^- \varphi_{j-,k+}^{n+1} + a_{jk}^+ b_{jk}^+ \varphi_{j-,k-}^{n+1}}{(a_{jk}^+ + a_{jk}^-)(b_{jk}^+ + b_{jk}^-)} \\ &- \frac{a_{jk}^+ a_{jk}^-}{b_{jk}^+ + b_{jk}^-}\left[b_{jk}^+ (\widehat{\varphi}_{xx})_{j,k-}^{n+1} + b_{jk}^- (\widehat{\varphi}_{xx})_{j,k+}^{n+1}\right]\frac{(\Delta t)^2}{2} \\ &- \frac{b_{jk}^+ b_{jk}^-}{a_{jk}^+ + a_{jk}^-}\left[a_{jk}^+ (\widehat{\varphi}_{yy})_{j-,k}^{n+1} + a_{jk}^- (\widehat{\varphi}_{yy})_{j+,k}^{n+1}\right]\frac{(\Delta t)^2}{2} + \mathcal{O}(\Delta t)^2. \end{aligned} \tag{3.7}$$

Substituting (3.3) into (3.7) yields

$$\begin{aligned}\varphi_{jk}^{n+1} &= \frac{a_{jk}^- b_{jk}^-}{(a_{jk}^+ + a_{jk}^-)(b_{jk}^+ + b_{jk}^-)}\Big(\widetilde{\varphi}_{j+,k+}^n - \Delta t \cdot H(\widetilde{\varphi}_x(x_{j+}^n, y_{k+}^n, t^n), \widetilde{\varphi}_y(x_{j+}^n, y_{k+}^n, t^n))\Big) \\ &+ \frac{a_{jk}^- b_{jk}^+}{(a_{jk}^+ + a_{jk}^-)(b_{jk}^+ + b_{jk}^-)}\Big(\widetilde{\varphi}_{j+,k-}^n - \Delta t \cdot H(\widetilde{\varphi}_x(x_{j+}^n, y_{k-}^n, t^n), \widetilde{\varphi}_y(x_{j+}^n, y_{k-}^n, t^n))\Big) \\ &+ \frac{a_{jk}^+ b_{jk}^-}{(a_{jk}^+ + a_{jk}^-)(b_{jk}^+ + b_{jk}^-)}\Big(\widetilde{\varphi}_{j-,k+}^n - \Delta t \cdot H(\widetilde{\varphi}_x(x_{j-}^n, y_{k+}^n, t^n), \widetilde{\varphi}_y(x_{j-}^n, y_{k+}^n, t^n))\Big) \\ &+ \frac{a_{jk}^+ b_{jk}^+}{(a_{jk}^+ + a_{jk}^-)(b_{jk}^+ + b_{jk}^-)}\Big(\widetilde{\varphi}_{j-,k-}^n - \Delta t \cdot H(\widetilde{\varphi}_x(x_{j-}^n, y_{k-}^n, t^n), \widetilde{\varphi}_y(x_{j-}^n, y_{k-}^n, t^n))\Big) \\ &- \frac{a_{jk}^+ a_{jk}^-}{b_{jk}^+ + b_{jk}^-}\left[b_{jk}^+ (\widehat{\varphi}_{xx})_{j,k-}^{n+1} + b_{jk}^- (\widehat{\varphi}_{xx})_{j,k+}^{n+1}\right]\frac{(\Delta t)^2}{2} \\ &- \frac{b_{jk}^+ b_{jk}^-}{a_{jk}^+ + a_{jk}^-}\left[a_{jk}^+ (\widehat{\varphi}_{yy})_{j-,k}^{n+1} + a_{jk}^- (\widehat{\varphi}_{yy})_{j+,k}^{n+1}\right]\frac{(\Delta t)^2}{2} + \mathcal{O}(\Delta t)^2. \end{aligned} \tag{3.8}$$

The values $\widetilde{\varphi}_{j\pm,k\pm}^n$ are computed by the Taylor expansions:

$$\widetilde{\varphi}_{j\pm,k\pm}^n = \varphi_{j,k}^n \pm \Delta t a_{jk}^{\pm} \varphi_x^{\pm} \pm \Delta t b_{jk}^{\pm} \varphi_y^{\pm} + \mathcal{O}(\Delta t)^2, \tag{3.9}$$

where $\varphi_x^{\pm} := \widetilde{\varphi}_x(x_j \pm 0, y_k, t^n)$ and $\varphi_y^{\pm} := \widetilde{\varphi}_y(x_j, y_k \pm 0, t^n)$ are the corresponding right and left derivatives of the continuous piecewise quadratic reconstruction at (x_j, y_k).

Next, substituting (3.9) into (3.8) gives

$$\begin{aligned}\varphi_{jk}^{n+1} &= \varphi_{jk}^n + \Delta t \frac{a_{jk}^+ a_{jk}^-}{a_{jk}^+ + a_{jk}^-}(\varphi_x^+ - \varphi_x^-) + \Delta t \frac{b_{jk}^+ b_{jk}^-}{b_{jk}^+ + b_{jk}^-}(\varphi_y^+ - \varphi_y^-) - \frac{\Delta t}{(a_{jk}^+ + a_{jk}^-)(b_{jk}^+ + b_{jk}^-)} \cdot \\ &\cdot \Big[a_{jk}^- b_{jk}^- H(\widetilde{\varphi}_x(x_{j+}^n, y_{k+}^n, t^n), \widetilde{\varphi}_y(x_{j+}^n, y_{k+}^n, t^n)) + a_{jk}^- b_{jk}^+ H(\widetilde{\varphi}_x(x_{j+}^n, y_{k-}^n, t^n), \widetilde{\varphi}_y(x_{j+}^n, y_{k-}^n, t^n)) \\ &+ a_{jk}^+ b_{jk}^- H(\widetilde{\varphi}_x(x_{j-}^n, y_{k+}^n, t^n), \widetilde{\varphi}_y(x_{j-}^n, y_{k+}^n, t^n)) + a_{jk}^+ b_{jk}^+ H(\widetilde{\varphi}_x(x_{j-}^n, y_{k-}^n, t^n), \widetilde{\varphi}_y(x_{j-}^n, y_{k-}^n, t^n))\Big] \\ &- \frac{a_{jk}^+ a_{jk}^-}{b_{jk}^+ + b_{jk}^-}\left[b_{jk}^+ (\widehat{\varphi}_{xx})_{j,k-}^{n+1} + b_{jk}^- (\widehat{\varphi}_{xx})_{j,k+}^{n+1}\right]\frac{(\Delta t)^2}{2} \\ &- \frac{b_{jk}^+ b_{jk}^-}{a_{jk}^+ + a_{jk}^-}\left[a_{jk}^+ (\widehat{\varphi}_{yy})_{j-,k}^{n+1} + a_{jk}^- (\widehat{\varphi}_{yy})_{j+,k}^{n+1}\right]\frac{(\Delta t)^2}{2} + \mathcal{O}(\Delta t)^2. \end{aligned} \tag{3.10}$$

Finally, the limit $\Delta t \to 0$ generates a family of 2-D *semi-discrete central-upwind schemes*:

$$\begin{aligned}\frac{d}{dt}\varphi_{jk}(t) &= -\frac{a^-_{jk}b^-_{jk}H(\varphi^+_x,\varphi^+_y)+a^-_{jk}b^+_{jk}H(\varphi^+_x,\varphi^-_y)+a^+_{jk}b^-_{jk}H(\varphi^-_x,\varphi^+_y)+a^+_{jk}b^+_{jk}H(\varphi^-_x,\varphi^-_y)}{(a^+_{jk}+a^-_{jk})(b^+_{jk}+b^-_{jk})}\\ &+\frac{a^+_{jk}a^-_{jk}}{a^+_{jk}+a^-_{jk}}\Big(\varphi^+_x-\varphi^-_x\Big)+\frac{b^+_{jk}b^-_{jk}}{b^+_{jk}+b^-_{jk}}\Big(\varphi^+_y-\varphi^-_y\Big)\\ &-\frac{a^+_{jk}a^-_{jk}}{b^+_{jk}+b^-_{jk}}\left[\frac{b^+_{jk}}{2}\lim_{\Delta t\to 0}\Big\{\Delta t(\widehat{\varphi}_{xx})^{n+1}_{j,k-}\Big\}+\frac{b^-_{jk}}{2}\lim_{\Delta t\to 0}\Big\{\Delta t(\widehat{\varphi}_{xx})^{n+1}_{j,k+}\Big\}\right]\\ &-\frac{b^+_{jk}b^-_{jk}}{a^+_{jk}+a^-_{jk}}\left[\frac{a^+_{jk}}{2}\lim_{\Delta t\to 0}\Big\{\Delta t(\widehat{\varphi}_{yy})^{n+1}_{j-,k}\Big\}+\frac{a^-_{jk}}{2}\lim_{\Delta t\to 0}\Big\{\Delta t(\widehat{\varphi}_{yy})^{n+1}_{j+,k}\Big\}\right].\end{aligned}\tag{3.11}$$

We still need to specify $(\widehat{\varphi}_{xx})^{n+1}_{j,k\pm}$ and $(\widehat{\varphi}_{yy})^{n+1}_{j\pm,k}$. If they are proportional to $(\Delta(\varphi_x))^{n+1}/\Delta x$ and to $(\Delta(\varphi_y))^{n+1}/\Delta y$ respectively, then

$$\lim_{\Delta t\to 0}\Big\{\Delta t(\widehat{\varphi}_{xx})^{n+1}_{j,k\pm}\Big\}=0,\quad \lim_{\Delta t\to 0}\Big\{\Delta t(\widehat{\varphi}_{yy})^{n+1}_{j\pm,k}\Big\}=0,$$

and we obtain the original 2-D central-upwind scheme from [10]. However, similarly to the 1-D case, we can choose $(\widehat{\varphi}_{xx})^{n+1}_{j,k\pm}$ and $(\widehat{\varphi}_{yy})^{n+1}_{j\pm,k}$ to be proportional to $1/\Delta t$, so that the above limit will not vanish. For example, one can use the minmod limiter:

$$\Delta t(\widehat{\varphi}_{xx})^{n+1}_{j,k\pm}=2\,\text{minmod}\left(\frac{(\widetilde{\varphi}_x)^{n+1}_{j+,k\pm}-\widetilde{\phi}_x(\widehat{x}^n_j,y^n_{k\pm},t^{n+1})}{a^+_{jk}+a^-_{jk}},\frac{\widetilde{\phi}_x(\widehat{x}^n_j,y^n_{k\pm},t^{n+1})-(\widetilde{\varphi}_x)^{n+1}_{j-,k\pm}}{a^+_{jk}+a^-_{jk}}\right),\tag{3.12}$$

$$\Delta t(\widehat{\varphi}_{yy})^{n+1}_{j\pm,k}=2\,\text{minmod}\left(\frac{(\widetilde{\varphi}_y)^{n+1}_{j\pm,k+}-\widetilde{\psi}_y(x_{j\pm},\widehat{y}_k,t^{n+1})}{b^+_{jk}+b^-_{jk}},\frac{\widetilde{\psi}_y(x_{j\pm},\widehat{y}_k,t^{n+1})-(\widetilde{\varphi}_y)^{n+1}_{j\pm,k-}}{b^+_{jk}+b^-_{jk}}\right),\tag{3.13}$$

where $(\widetilde{\varphi}_x)^{n+1}_{j\pm,k\pm}:=\widetilde{\varphi}_x(x^n_{j\pm},y^n_{k\pm},t^{n+1})$ and $(\widetilde{\varphi}_y)^{n+1}_{j\pm,k\pm}:=\widetilde{\varphi}_y(x^n_{j\pm},y^n_{k\pm},t^{n+1})$. The values of the derivative $\widetilde{\phi}_x$ in (3.12) are given by

$$\widetilde{\phi}_x(\widehat{x}^n_j,y^n_{k\pm},t^{n+1})=\frac{\varphi^{n+1}_{j+,k\pm}-\varphi^{n+1}_{j-,k\pm}}{(a^+_{jk}+a^-_{jk})\Delta t},\tag{3.14}$$

and after using (3.3) and (3.9), we obtain

$$\begin{aligned}\widetilde{\phi}_x(\widehat{x}^n_j,y^n_{k\pm},t^{n+1}) &= -\frac{H(\widetilde{\varphi}_x(x^n_{j+},y^n_{k\pm},t^n),\widetilde{\varphi}_y(x^n_{j+},y^n_{k\pm},t^n))-H(\widetilde{\varphi}_x(x^n_{j-},y^n_{k\pm},t^n),\widetilde{\varphi}_y(x^n_{j-},y^n_{k\pm},t^n))}{(a^+_{jk}+a^-_{jk})}\\ &+\frac{a^+_{jk}\varphi^+_x+a^-_{jk}\varphi^-_x}{(a^+_{jk}+a^-_{jk})}+\mathcal{O}(\Delta t).\end{aligned}\tag{3.15}$$

Since the data is smooth along the line segments $(x^n_{j\pm},y^n_{k\pm},t)$, $t^n\le t<t^{n+1}$, it is clear that

$$\lim_{\Delta t\to 0}(\varphi_x)^{n+1}_{j+,k\pm}=\varphi^+_x,\ \lim_{\Delta t\to 0}(\varphi_x)^{n+1}_{j-,k\pm}=\varphi^-_x,\ \lim_{\Delta t\to 0}(\varphi_y)^{n+1}_{j\pm,k+}=\varphi^+_y,\ \lim_{\Delta t\to 0}(\varphi_y)^{n+1}_{j\pm,k-}=\varphi^-_y.\tag{3.16}$$

Therefore using (3.12), (3.16), and (3.15), we obtain

$$\lim_{\Delta t\to 0}\Big\{\Delta t(\widehat{\varphi}_{xx})^{n+1}_{j,k\pm}\Big\}=\frac{2}{(a^+_{jk}+a^-_{jk})}\,\text{minmod}\Big(\varphi^+_x-\varphi^{\text{int}\pm}_x,\varphi^{\text{int}\pm}_x-\varphi^-_x\Big),\tag{3.17}$$

where

$$\varphi_x^{\text{int}\pm} := \frac{a_{jk}^+\varphi_x^+ + a_{jk}^-\varphi_x^-}{(a_{jk}^+ + a_{jk}^-)} - \frac{H(\varphi_x^+,\varphi_y^\pm) - H(\varphi_x^-,\varphi_y^\pm)}{(a_{jk}^+ + a_{jk}^-)}. \tag{3.18}$$

Likewise, using (3.13), we obtain

$$\lim_{\Delta t\to 0}\left\{\Delta t(\widehat{\varphi}_{yy})_{j\pm,k}^{n+1}\right\} = \frac{2}{(b_{jk}^+ + b_{jk}^-)}\,\text{minmod}\left(\varphi_y^+ - \varphi_y^{\text{int}\pm},\ \varphi_y^{\text{int}\pm} - \varphi_y^-\right), \tag{3.19}$$

where

$$\varphi_y^{\text{int}\pm} := \frac{b_{jk}^+\varphi_y^+ + b_{jk}^-\varphi_y^-}{(b_{jk}^+ + b_{jk}^-)} - \frac{H(\varphi_x^\pm,\varphi_y^+) - H(\varphi_x^\pm,\varphi_y^-)}{(b_{jk}^+ + b_{jk}^-)}. \tag{3.20}$$

Finally, we substitute (3.17) and (3.19) into (3.11). The resulting 2-D *compressed semi-discrete central-upwind scheme* is

$$\begin{aligned}
\frac{d}{dt}\varphi_{jk}(t) \;=\; & -\frac{a_{jk}^-b_{jk}^-H(\varphi_x^+,\varphi_y^+) + a_{jk}^-b_{jk}^+H(\varphi_x^+,\varphi_y^-) + a_{jk}^+b_{jk}^-H(\varphi_x^-,\varphi_y^+) + a_{jk}^+b_{jk}^+H(\varphi_x^-,\varphi_y^-)}{(a_{jk}^+ + a_{jk}^-)(b_{jk}^+ + b_{jk}^-)} \\
& + a_{jk}^+a_{jk}^-\left[\frac{\varphi_x^+ - \varphi_x^-}{a_{jk}^+ + a_{jk}^-} - \frac{b_{jk}^+}{b_{jk}^+ + b_{jk}^-}\,\text{minmod}\left(\frac{\varphi_x^+ - \varphi_x^{\text{int}-}}{a_{jk}^+ + a_{jk}^-},\ \frac{\varphi_x^{\text{int}-} - \varphi_x^-}{a_{jk}^+ + a_{jk}^-}\right)\right. \\
& \left. - \frac{b_{jk}^-}{b_{jk}^+ + b_{jk}^-}\,\text{minmod}\left(\frac{\varphi_x^+ - \varphi_x^{\text{int}+}}{a_{jk}^+ + a_{jk}^-},\ \frac{\varphi_x^{\text{int}+} - \varphi_x^-}{a_{jk}^+ + a_{jk}^-}\right)\right] \\
& + b_{jk}^+b_{jk}^-\left[\frac{\varphi_y^+ - \varphi_y^-}{b_{jk}^+ + b_{jk}^-} - \frac{a_{jk}^+}{a_{jk}^+ + a_{jk}^-}\,\text{minmod}\left(\frac{\varphi_y^+ - \varphi_y^{\text{int}-}}{b_{jk}^+ + b_{jk}^-},\ \frac{\varphi_y^{\text{int}-} - \varphi_y^-}{b_{jk}^+ + b_{jk}^-}\right)\right. \\
& \left. - \frac{a_{jk}^-}{a_{jk}^+ + a_{jk}^-}\,\text{minmod}\left(\frac{\varphi_y^+ - \varphi_y^{\text{int}+}}{b_{jk}^+ + b_{jk}^-},\ \frac{\varphi_y^{\text{int}+} - \varphi_y^-}{b_{jk}^+ + b_{jk}^-}\right)\right].
\end{aligned} \tag{3.21}$$

Here, $\varphi_x^{\text{int}\pm}$ and $\varphi_y^{\text{int}\pm}$ are given by (3.18) and (3.20), respectively; the one-sided local speeds, $a_{jk}^\pm$ and $b_{jk}^\pm$, are given by (3.2); and formulas for $\varphi_x^\pm$ and $\varphi_y^\pm$ are discussed in §3.3 below.

Remark. In practice, for convex Hamiltonians H the one-sided local speeds are computed as

$$\begin{aligned}
a_{jk}^+ &= \max_\pm\left\{H_x\left(\varphi_x^\pm,\varphi_y^\pm\right),0\right\}, \quad a_{jk}^- = \left|\min_\pm\left\{H_x\left(\varphi_x^\pm,\varphi_y^\pm\right),0\right\}\right|, \\
b_{jk}^+ &= \max_\pm\left\{H_y\left(\varphi_x^\pm,\varphi_y^\pm\right),0\right\}, \quad b_{jk}^- = \left|\min_\pm\left\{H_y\left(\varphi_x^\pm,\varphi_y^\pm\right),0\right\}\right|,
\end{aligned} \tag{3.22}$$

where the maximum and minimum are taken over all the possible permutations of $\pm$.

3.2 A Three-Dimensional Scheme

We consider the three-dimensional (3-D) Hamilton-Jacobi equation,

$$\varphi_t + H(\varphi_x,\varphi_y,\varphi_z) = 0.$$

We use the maximal values of the one-sided local speeds of propagation, $a_{jkl}^\pm, b_{jkl}^\pm$, and $c_{jkl}^\pm$, in the x-, y- and z-directions, respectively. These values at any grid point (x_j,y_k,z_l) are given by the obvious generalizations of (3.2) and

$$c_{jkl}^+ := \max_{C_{jkl}}\left\{H_w(\widetilde{\varphi}_x(x,y,z,t),\widetilde{\varphi}_y(x,y,z,t),\widetilde{\varphi}_z(x,y,z,t))\right\}_+,$$

$$c^-_{jkl} := \left|\min_{C_{jkl}}\left\{H_w(\widetilde{\varphi}_x(x,y,z,t),\widetilde{\varphi}_y(x,y,z,t),\widetilde{\varphi}_z(x,y,z,t))\right\}_-\right|,$$

where $C_{jkl} := [x_{j-\frac12},x_{j+\frac12}]\times[y_{k-\frac12},y_{k+\frac12}]\times,[z_{l-\frac12},z_{l+\frac12}]$. Proceeding as in two dimensions, the 3-D *compressed semi-discrete central-upwind scheme* is (suppressing the indices j,k,l)

$$\begin{aligned}\frac{d\varphi}{dt} &= -\frac{1}{(a^++a^-)(b^++b^-)(c^++c^-)}\sum_{\pm}\left[a^\pm b^\pm c^\pm H(\varphi_x^\mp,\varphi_y^\mp,\varphi_z^\mp)\right]\\ &+\frac{a^+a^-}{a^++a^-}\left(\varphi_x^+-\varphi_x^-\right)+\frac{b^+b^-}{b^++b^-}\left(\varphi_y^+-\varphi_y^-\right)+\frac{c^+c^-}{c^++c^-}\left(\varphi_z^+-\varphi_z^-\right)\\ &-\frac{1}{(a^++a^-)(b^++b^-)(c^++c^-)}\Bigg\{a^+a^-\sum_{\pm}\left[b^\pm c^\pm(D_x^2\varphi)^{n+1}_{j,k\mp,l\mp}\right]\\ &+b^+b^-\sum_{\pm}\left[a^\pm c^\pm(D_y^2\varphi)^{n+1}_{j\mp,k,l\mp}\right]+c^+c^-\sum_{\pm}\left[a^\pm b^\pm(D_z^2\varphi)^{n+1}_{j\mp,k\mp,l}\right]\Bigg\},\end{aligned}\tag{3.23}$$

where the summations are taken over all possible permutations of $+$ and $-$. For example, in the first sum $a^+b^-c^+$ should be multiplied by $H(\varphi_x^-,\varphi_y^+,\varphi_z^-)$. In (3.23), we use the notation

$$(D_x^2\varphi)^{n+1}_{j,k\pm,l\pm} := \text{minmod}\left(\varphi_x^+-(\varphi_x^{\text{int}})_{j,k\pm,l\pm},(\varphi_x^{\text{int}})_{j,k\pm,l\pm}-\varphi_x^-\right),$$

$$(D_y^2\varphi)^{n+1}_{j\pm,k,l\pm} := \text{minmod}\left(\varphi_y^+-(\varphi_y^{\text{int}})_{j\pm,k,l\pm},(\varphi_y^{\text{int}})_{j\pm,k,l\pm}-\varphi_y^-\right),$$

$$(D_z^2\varphi)^{n+1}_{j\pm,k\pm,l} := \text{minmod}\left(\varphi_z^+-(\varphi_z^{\text{int}})_{j\pm,k\pm,l},(\varphi_z^{\text{int}})_{j\pm,k\pm,l}-\varphi_z^-\right),$$

where

$$(\varphi_x^{\text{int}})_{j,k\pm,l\pm} := \frac{a^+\varphi_x^+ + a^-\varphi_x^-}{(a^++a^-)} - \frac{H(\varphi_x^+,\varphi_y^\pm,\varphi_z^\pm)-H(\varphi_x^-,\varphi_y^\pm,\varphi_z^\pm)}{(a^++a^-)},$$

$$(\varphi_y^{\text{int}})_{j\pm,k,l\pm} := \frac{b^+\varphi_y^+ + b^-\varphi_y^-}{(b^++b^-)} - \frac{H(\varphi_x^\pm,\varphi_y^+,\varphi_z^\pm)-H(\varphi_x^\pm,\varphi_y^-,\varphi_z^\pm)}{(b^++b^-)},$$

$$(\varphi_z^{\text{int}})_{j\pm,k\pm,l} := \frac{c^+\varphi_z^+ + c^-\varphi_z^-}{(c^++c^-)} - \frac{H(\varphi_x^\pm,\varphi_y^\pm,\varphi_z^+)-H(\varphi_x^\pm,\varphi_y^\pm,\varphi_z^-)}{(c^++c^-)}.$$

3.3 Multidimensional Interpolants

The schemes developed in §3.1–3.2 require a multidimensional non-oscillatory reconstruction. The simplest option is to use straightforward multidimensional extensions of the 1-D interpolants from §2.2–2.3, obtained via a "dimension-by-dimension" approach.

For example, a 2-D non-oscillatory second-order central-upwind scheme is given by (3.21) with

$$\varphi_x^\pm = \frac{(\Delta\varphi)^n_{j\pm\frac12,k}}{\Delta x}\mp\frac{\Delta x}{2}(\varphi_{xx})^n_{j+\frac12,k},\quad \varphi_y^\pm = \frac{(\Delta\varphi)^n_{j,k\pm\frac12}}{\Delta y}\mp\frac{\Delta y}{2}(\varphi_{yy})^n_{j,k+\frac12},$$

$$(\varphi_{xx})^n_{j+\frac12,k} = \text{minmod}\left(\theta\frac{(\Delta\varphi)^n_{j+\frac32,k}-(\Delta\varphi)^n_{j+\frac12,k}}{(\Delta x)^2},\frac{(\Delta\varphi)^n_{j+\frac32,k}-(\Delta\varphi)^n_{j-\frac12,k}}{2(\Delta x)^2},\theta\frac{(\Delta\varphi)^n_{j+\frac12,k}-(\Delta\varphi)^n_{j-\frac12,k}}{(\Delta x)^2}\right),$$

$$(\varphi_{yy})^n_{j,k+\frac{1}{2}} = \text{minmod}\left(\theta\frac{(\Delta\varphi)^n_{j,k+\frac{3}{2}} - (\Delta\varphi)^n_{j,k+\frac{1}{2}}}{(\Delta x)^2}, \frac{(\Delta\varphi)^n_{j,k+\frac{3}{2}} - (\Delta\varphi)^n_{j,k-\frac{1}{2}}}{2(\Delta x)^2}, \theta\frac{(\Delta\varphi)^n_{j,k+\frac{1}{2}} - (\Delta\varphi)^n_{j,k-\frac{1}{2}}}{(\Delta x)^2}\right),$$

where $\theta \in [1,2]$, and the minmod function is given by (2.12). Similarly, the corresponding "dimension-by-dimension" 2-D extensions of the WENO interpolants from §2.3 can be used to reconstruct the derivatives in (3.18), (3.20), and (3.21). For more details see [4].

4 Numerical Examples

In this section, we test the performance of the new compressed semi-discrete central-upwind schemes on a variety of numerical examples. We compare the methods developed in this paper, labeled BKLP, with the second-order scheme from [10] and the fifth-order scheme from [4], both of which are referred to as KNP. Our results demonstrate that the BKLP schemes achieve a better resolution of singularities in comparison with the corresponding KNP schemes.

Note that in regions where the solution is sufficiently smooth, a^+a^- and b^+b^- are either equal to zero or very small (for smooth Hamiltonians and sufficiently small Δx and Δy). Hence, the BKLP and KNP schemes of the same order will be almost identical in these areas, and thus there will be practically no difference in the resolution of smooth solutions. We therefore only examine results after the formation of singularities, for which a^+a^- and/or b^+b^- may be large.

4.1 One-Dimensional Problems

A Convex Hamiltonian

We first test the performance of our schemes for the Hamilton-Jacobi equation with a convex Hamiltonian:

$$\varphi_t + \frac{1}{2}(\varphi_x + 1)^2 = 0, \tag{4.1}$$

subject to the periodic initial data $\varphi(x,0) = -\cos(\pi x)$. The change of variables $u(x,t) = \varphi_x(x,t) + 1$ transforms the equation into the Burgers equation $u_t + \frac{1}{2}(u^2)_x = 0$, which can be easily solved via the method of characteristics. The solution develops a singularity in the form of a discontinuous derivative at time $t = 1/\pi^2$.

The computed solutions at $T = 2.5/\pi^2$ (after the singularity formation) are shown in Figure 5.1, where the second- and fifth-order BKLP and KNP schemes are compared. There is significant improvement in the resolution of the singularity for the BKLP schemes compared with the KNP schemes. The second-order BKLP scheme has a smaller error at the singularity than the fifth-order KNP scheme, while the fifth-order BKLP scheme has the smallest error. In Table 5.1 we show the relative L^1- and L^∞-errors.

A Non-Convex Hamiltonian

In this example, we compute the solution of the 1-D Hamilton-Jacobi equation with a non-convex Hamiltonian:

$$\varphi_t - \cos(\varphi_x + 1) = 0, \tag{4.2}$$

subject to the periodic initial data $\varphi(x,0) = -\cos(\pi x)$. This initial-value problem has a smooth solution for $t \lesssim 1.049/\pi^2$, after which a singularity forms. A second singularity forms at $t \approx 1.29/\pi^2$. The solutions at time $T = 2/\pi^2$, computed with $N = 100$, are shown in Figure 5.2, with a close-up of the singularities in Figure 5.3. The convergence results before and after the singularity formation

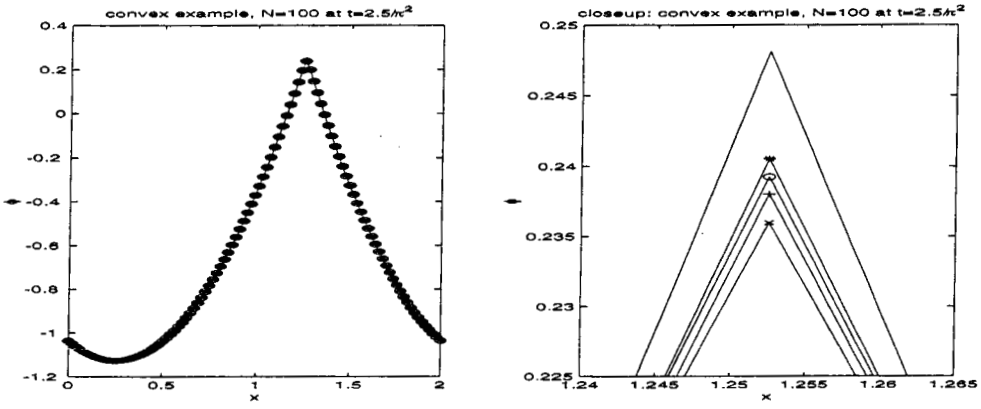

Figure 5.1: Problem (4.1). *Left:* The solution. *Right:* A close-up of the solution near the singularity. "×": 2nd-order KNP, "o": 2nd-order BKLP, "+": 5th-order KNP, "∗": 5th-order BKLP, "–": exact solution.

	Convex example $\varphi_t + \frac{1}{2}(\varphi_x + 1)^2 = 0$			
	2nd-order after singularity $T = 2.5/\pi^2$			
	relative L^1*-error*		*relative* L^∞*-error*	
N	*KNP*	*BKLP*	*KNP*	*BKLP*
100	3.43×10^{-4}	2.94×10^{-4}	1.76×10^{-4}	1.29×10^{-4}
200	4.57×10^{-5}	4.10×10^{-5}	7.00×10^{-6}	1.96×10^{-6}
400	2.15×10^{-5}	1.85×10^{-5}	1.18×10^{-5}	8.85×10^{-6}
800	2.87×10^{-6}	2.55×10^{-6}	4.38×10^{-7}	1.47×10^{-7}
	5th-order after singularity $T = 2.5/\pi^2$			
	relative L^1*-error*		*relative* L^∞*-error*	
N	*KNP*	*BKLP*	*KNP*	*BKLP*
100	1.50×10^{-4}	1.13×10^{-4}	1.46×10^{-4}	1.10×10^{-4}
200	2.33×10^{-6}	9.95×10^{-7}	1.56×10^{-6}	3.42×10^{-7}
400	9.39×10^{-6}	7.08×10^{-6}	9.33×10^{-6}	7.02×10^{-6}
800	1.13×10^{-7}	3.94×10^{-8}	7.54×10^{-8}	1.41×10^{-8}

Table 5.1: Problem (4.1). Relative L^1- and L^∞-errors for the KNP and BKLP schemes.

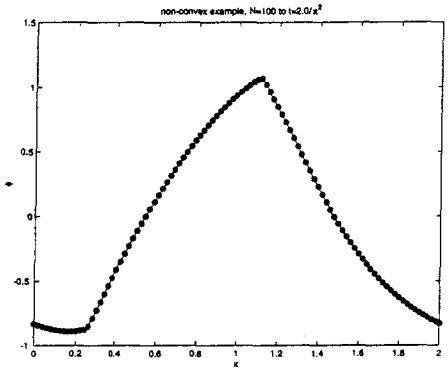

Figure 5.2: Problem (4.2) — the KNP and BKLP numerical solutions.

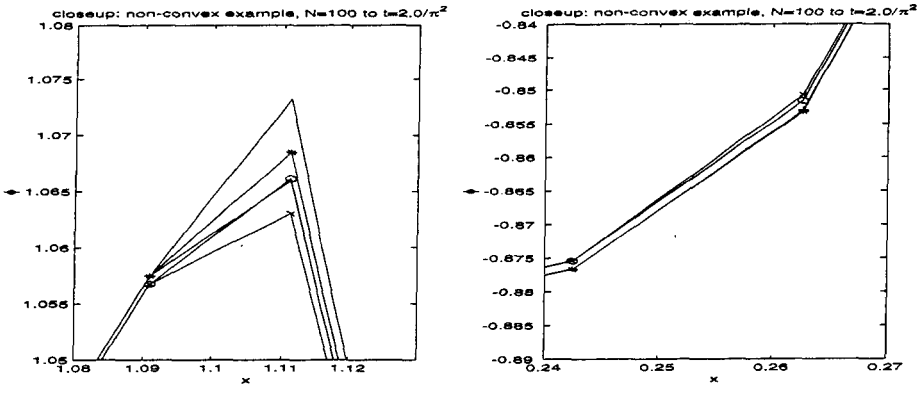

Figure 5.3: Problem (4.2). *Left:* The singularity near $x = 0.25$. *Right:* The singularity near $x = 1.11$. "×": 2nd-order KNP, "o": 2nd-order BKLP, "+": 5th-order KNP, "∗": 5th-order BKLP, "−": exact solution.

are given in Table 5.2. In this example, the local speeds of propagation were estimated by (2.2). The results are similar to the convex case, though the improvement here is somewhat less dramatic.

Next, we examine the convergence of the numerical solutions of (4.1) and (4.2), computed by the fifth-order BKLP and KNP schemes. These results, together with the fifth-order methods from [7] and [3], are shown in Figure 5.4. The reader may note that the convergence rates in these examples are erratic. However, this investigation of the relative L^1-errors for many different grid spacings shows that the behavior is due to super-convergence at some grid spacings. Notice that for all grid spacings the L^1-error of the BKLP method is less than the others.

4.2 Two-Dimensional Problems

In this section, we test the 2-D BKLP schemes on Hamilton-Jacobi equations with convex and non-convex Hamiltonians. We start with the convex problem (compare with (4.1)):

$$\varphi_t + \frac{1}{2}\left(\varphi_x + \varphi_y + 1\right)^2 = 0, \tag{4.3}$$

	Non-convex example $\varphi_t - \cos(\varphi_x + 1) = 0$			
	2nd-order after singularity $T = 2.0/\pi^2$			
	relative L^1*-error*		*relative* L^∞*-error*	
N	*KNP*	*BKLP*	*KNP*	*BKLP*
100	5.59×10^{-4}	4.97×10^{-4}	1.75×10^{-4}	1.22×10^{-4}
200	9.52×10^{-5}	9.52×10^{-5}	4.47×10^{-6}	4.11×10^{-6}
400	2.40×10^{-5}	2.40×10^{-5}	2.06×10^{-6}	1.57×10^{-6}
800	6.02×10^{-6}	6.02×10^{-6}	6.30×10^{-7}	3.09×10^{-7}
	5th-order after singularity $T = 2.0/\pi^2$			
	relative L^1*-error*		*relative* L^∞*-error*	
N	*KNP*	*BKLP*	*KNP*	*BKLP*
100	1.48×10^{-4}	9.91×10^{-5}	1.25×10^{-4}	8.17×10^{-5}
200	8.49×10^{-8}	5.82×10^{-8}	1.35×10^{-7}	8.88×10^{-8}
400	7.89×10^{-9}	6.60×10^{-9}	8.21×10^{-7}	5.48×10^{-7}
800	6.63×10^{-10}	5.13×10^{-10}	2.25×10^{-7}	7.77×10^{-8}

Table 5.2: Problem (4.2). Relative L^1- and L^∞-errors for the KNP and BKLP schemes.

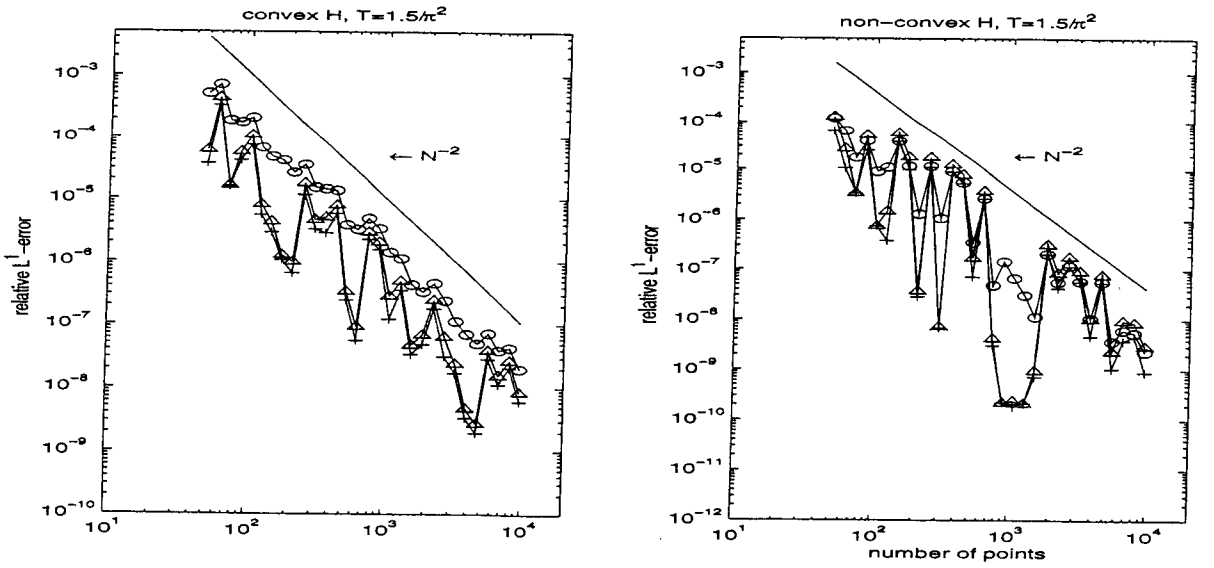

Figure 5.4: Convergence of the 1-D examples. *Left:* Problem (4.1), $T = 2.5/\pi^2$. *Right:* Problem (4.1), $T = 2/\pi^2$. "+": 5th-order BKLP, "△": 5th-order KNP, "o": the 5th-order method from [7], The solid lines show example rates of convergence.

which can be reduced to a 1-D problem via the coordinate transformation

$$\begin{pmatrix} \xi \\ \eta \end{pmatrix} = \begin{pmatrix} 1/2 & 1/2 \\ 1/2 & -1/2 \end{pmatrix} \begin{pmatrix} x \\ y \end{pmatrix}.$$

The relative L^1- and L^∞-errors for the periodic initial data $\varphi(x,y,0) = -\cos(\pi(x+y)/2) = -\cos(\pi\xi)$ after the singularity formation at $T = 2.5/\pi^2$ are shown in Table 5.3.

	2-D Convex example			
	2nd-order after singularity $T = 2.5/\pi^2$			
	relative L^1*-error*		*relative* L^∞*-error*	
N	*KNP*	*BKLP*	*KNP*	*BKLP*
50	7.31×10^{-4}	7.26×10^{-4}	2.13×10^{-6}	2.23×10^{-6}
100	3.27×10^{-4}	2.99×10^{-4}	1.58×10^{-6}	1.30×10^{-6}
200	4.37×10^{-5}	4.12×10^{-5}	2.34×10^{-8}	9.87×10^{-9}
	5th-order after singularity $T = 2.5/\pi^2$			
	relative L^1*-error*		*relative* L^∞*-error*	
N	*KNP*	*BKLP*	*KNP*	*BKLP*
50	6.01×10^{-5}	4.39×10^{-4}	3.79×10^{-7}	1.60×10^{-7}
100	1.40×10^{-4}	1.19×10^{-4}	1.33×10^{-6}	1.11×10^{-6}
200	1.98×10^{-6}	1.23×10^{-6}	5.97×10^{-9}	2.58×10^{-9}

Table 5.3: Problem (4.3). Relative L^1- and L^∞-errors for the 2-D KNP and BKLP schemes.

In Table 5.4, we present similar results for the non-convex problem (compare with (4.2)):

$$\varphi_t - \cos(\varphi_x + \varphi_y + 1) = 0, \tag{4.4}$$

with the periodic initial data $\varphi(x,y,0) = -\cos(\pi(x+y)/2)$.

	2-D non-convex example			
	2nd-order after singularity $T = 2.0/\pi^2$			
	relative L^1*-error*		*relative* L^∞*-error*	
N	*KNP*	*BKLP*	*KNP*	*BKLP*
50	1.84×10^{-3}	1.75×10^{-3}	5.11×10^{-6}	3.66×10^{-6}
100	5.86×10^{-4}	5.48×10^{-4}	1.50×10^{-6}	1.21×10^{-6}
200	1.14×10^{-4}	1.13×10^{-4}	2.15×10^{-8}	2.04×10^{-8}
	5th-order after singularity $T = 2.0/\pi^2$			
	relative L^1*-error*		*relative* L^∞*-error*	
N	*KNP*	*BKLP*	*KNP*	*BKLP*
50	1.79×10^{-4}	1.44×10^{-4}	6.81×10^{-7}	6.80×10^{-7}
100	1.14×10^{-4}	8.97×10^{-5}	1.02×10^{-6}	7.82×10^{-7}
200	4.42×10^{-7}	4.32×10^{-7}	5.65×10^{-10}	4.18×10^{-10}

Table 5.4: Problem (4.4). Relative L^1- and L^∞-errors for the 2-D KNP and BKLP schemes.

A Appendix: A Proof of Theorem 2.1

Proof. First, we fix u^- and show that $H^{BKLP}(u,u^-)$ given by (2.22) is a non-increasing function of u (the proof that H^{BKLP} is non-decreasing function of its second argument is similar). We denote by

$$Q(u) := \begin{cases} \dfrac{H(u)-H(u^-)}{u-u^-}, & u \neq u^-, \\ \\ H'(u^-), & u = u^-, \end{cases} \tag{A.1}$$

and

$$A(u) := \frac{1}{2}\left(a^+(u) - a^-(u)\right),$$

where $a^+(u) = \max\{H'(u), H'(u^-), 0\}$ and $a^-(u) = |\min\{H'(u), H'(u^-), 0\}|$, and by U_1, U_2, V_1, V_2, the sets

$$U_1 := U_1(u^-) = \{u : Q(u) - A(u) < 0\}, \quad U_2 := U_2(u^-) = \{u : Q(u) - A(u) \geq 0\}, \tag{A.2}$$

$$V_1 := V_1(u^-) = \{u : Q(u) - A(u) \leq 0\}, \quad V_2 := V_2(u^-) = \{u : Q(u) - A(u) > 0\}. \tag{A.3}$$

Both U_1 and V_2 are open sets (Q and A are continuous) and as such can be represented as a union of at most countably many disjoint open intervals I_j and J_j, respectively, i.e.

$$U_1 = \cup_{j=1}^{\infty} I_j \quad \text{and} \quad V_2 = \cup_{j=1}^{\infty} J_j. \tag{A.4}$$

In the new notation it is easy to verify that the Hamiltonian H^{BKLP} can be written as

$$H^{BKLP}(u,u^-) := \begin{cases} H_1^{BKLP}(u,u^-), & u \in U_1, \\ \\ H_2^{BKLP}(u,u^-), & u \in U_2, \end{cases} \tag{A.5}$$

or as

$$H^{BKLP}(u,u^-) := \begin{cases} H_1^{BKLP}(u,u^-), & u \in V_1, \\ \\ H_2^{BKLP}(u,u^-), & u \in V_2, \end{cases} \tag{A.6}$$

where

$$\begin{aligned} H_1^{BKLP}(u,u^-) &:= \frac{a^-(u)H(u^+) + a^+(u)H(u^-)}{a^+(u)+a^-(u)} - \frac{a^+(u)a^-(u)}{a^+(u)+a^-(u)}(u-u^-) \\ &+ \frac{a^+(u)a^-(u)}{(a^+(u)+a^-(u))^2}(u-u^-)\left[Q(u)+a^-(u)\right], \end{aligned} \tag{A.7}$$

and

$$\begin{aligned} H_2^{BKLP}(u,u^-) &:= \frac{a^-(u)H(u^+) + a^+(u)H(u^-)}{a^+(u)+a^-(u)} - \frac{a^+(u)a^-(u)}{a^+(u)+a^-(u)}(u-u^-) \\ &+ \frac{a^+(u)a^-(u)}{(a^+(u)+a^-(u))^2}(u-u^-)\left[a^+(u)-Q(u)\right]. \end{aligned} \tag{A.8}$$

Notice that for those u for which $Q(u) = A(u)$, we have that $H_1^{BKLP}(u,u^-) = H_2^{BKLP}(u,u^-)$, and therefore $H^{BKLP}(\cdot,u^-)$ is a well defined function consisting of the pieces $H_i^{BKLP}(\cdot,u^-)$, $i=1,2$. We will

use formulas (A.5) and (A.6) and continuity arguments to show that $H^{BKLP}(\cdot, u^-)$ is a non-increasing function on the whole real line.

Consider the point u^* such that $H'(u^*) = 0$ (see assumption $(A1)$). Then $H_i^{BKLP}(u, u^-)$, $i = 1, 2$, are continuously differentiable on the intervals $(-\infty, \min(u^-, u^*))$, $(\min(u^-, u^*), \max(u^-, u^*))$, and $(\max(u^-, u^*), \infty)$ (in case $u^- = u^*$, on the first and third interval only) and continuous on $\mathbb{R}$.

Case 1. Let $u \in (-\infty, \min(u^-, u^*))$. Then $\frac{d}{du}(a^+(u)) = 0$ since $a^+(u) = \max\{H'(u), H'(u^-), 0\}$ and H' is a non-decreasing function of u. In this case we have

$$\frac{d}{du}\left(H_2^{BKLP}(u, u^-)\right) = - \frac{2(a^-(u))' a^-(u) a^+(u)(u - u^-)}{(a^+(u) + a^-(u))^3}\left[a^+(u) - Q(u)\right] - \frac{(a^-(u))^2(a^+(u) - H'(u))}{(a^+(u) + a^-(u))^2}.$$

Note that there exists $\xi \in (u, u^-)$ such that

$$Q(u) := \frac{H(u) - H(u^-)}{u - u^-} = H'(\xi) \le H'(u^-) \le a^+(u),$$

a^- is a smooth non-increasing function on $(-\infty, \min(u^-, u^*))$, $a^+(u) \ge 0$, $a^-(u) \ge 0$, $H'(u) \le a^+(u)$, and therefore the derivative $\frac{d}{du}\left(H_2^{BKLP}(u, u^-)\right) \le 0$. Hence $H_2^{BKLP}(u, u^-)$ is non-increasing on $(-\infty, \min(u^-, u^*))$.

Similarly, for $u \in (-\infty, \min(u^-, u^*))$ we have

$$\frac{d}{du}\left(H_1^{BKLP}(u, u^-)\right) = \frac{2(a^-(u))'(a^+(u))^2(u - u^-)}{(a^+(u) + a^-(u))^3}\left[Q(u) - A(u)\right] - \frac{a^-(u)a^+(u)(a^+(u) - H'(u))}{(a^+(u) + a^-(u))^2} + \frac{a^-(u)H'(u)}{a^+(u) + a^-(u)}. \tag{A.9}$$

Now we fix j and consider the corresponding open interval $I_j \cap (-\infty, \min(u^-, u^*))$ (see (A.4) and representation (A.5)). As above, a^- is a smooth non-increasing function on $(-\infty, \min(u^-, u^*))$, $a^+(u) \ge 0$, $a^-(u) \ge 0$. On each I_j, $Q(u) < A(u)$, and therefore the first term on the right-hand side (RHS) of (A.9) ≤ 0. The second term is non-positive since $a^+(u) \ge H'(u)$. The last term is ≤ 0 because $H'(u) \le 0$ for $u \in (-\infty, \min(u^-, u^*))$. This proves that $H_1^{BKLP}(u, u^-)$ is a non-increasing function of u on $I_j \cap (-\infty, \min(u^-, u^*))$, for every j.

Case 2. Let $u \in (\min(u^-, u^*), \max(u^-, u^*))$. In this case the derivatives are $\frac{d}{du}(a^+(u)) = 0$ and $\frac{d}{du}(a^-(u)) = 0$. Therefore

$$\frac{d}{du}\left(H_2^{BKLP}(u, u^-)\right) = -\frac{(a^-(u))^2(a^+(u) - H'(u))}{(a^+(u) + a^-(u))^2} \le 0, \quad \text{since} \quad a^+(u) \ge H'(u),$$

which shows that $H_2^{BKLP}(\cdot, u^-)$ is non-increasing on $(\min(u^-, u^*), \max(u^-, u^*))$. Likewise

$$\frac{d}{du}\left(H_1^{BKLP}(u, u^-)\right) = -\frac{a^-(u)a^+(u)(a^+(u) - H'(u))}{(a^+(u) + a^-(u))^2} + \frac{a^-(u)H'(u)}{a^+(u) + a^-(u)}.$$

The first term on the RHS is ≤ 0 since $a^+(u) \ge H'(u)$. As for the second term, we have two possibilities. If $u^- < u < u^*$ then $H'(u) < 0$, which will make the whole term ≤ 0. If $u^* < u < u^-$, then $a^-(u) \equiv 0$ and the second term is 0. Therefore, the derivative of H_1^{BKLP} is ≤ 0, and thus $H_1^{BKLP}(\cdot, u^-)$ is non-increasing on $(\min(u^-, u^*), \max(u^-, u^*))$, and in particular on $I_j \cap (\min(u^-, u^*), \max(u^-, u^*))$ for every j.

Case 3a. Let $u^* \le u^- \le u$. Then $a^-(u) \equiv 0$ and therefore $H^{BKLP} \equiv H_1^{BKLP}(u,u^-) \equiv H_2^{BKLP}(u,u^-) \equiv H(u^-)$. In particular, H_2^{BKLP} is a non-increasing function on (u^-,∞), and H_1^{BKLP} is a non-increasing function on $I_j \cap (u^-,\infty)$, for every j.

Combining the results from Cases 1, 2 and 3a, we obtain that H_2^{BKLP} is non-increasing on the whole real line (since it is continuous on $\mathbb{R}$ and non-increasing on each of the intervals $(-\infty,\min(u^-,u^*))$, $(\min(u^-,u^*),\max(u^-,u^*))$, and $(\max(u^-,u^*),\infty))$, and H_1^{BKLP} is a non-increasing function on every open interval I_j from U_1 (same reasoning). Since $H_2^{BKLP}(u,u^-) = H_1^{BKLP}(u,u^-)$ for $u \in \partial I_j$ it will follow from (A.5) that $H^{BKLP}(\cdot,u^-)$ is non-increasing on the whole real line.

Case 3b. Let $u^- \le u^* \le u$. In this case we will utilize representation (A.6) for H^{BKLP} and, using the results from Cases 1 and 2, we will show that H^{BKLP} is a non-increasing function on the interval $[a,b]$ for any a and b, and therefore on the whole real line.

Notice that in this case $V_1 \equiv S^-(u,u^-)$, and then, by assumption *(A2)*, $V_1 \cap [a,b]$ is either $\varnothing$ or a finite number of points and/or a finite union of closed intervals $\mathcal{T}_k$. Note also that we have

$$(u^*,\infty) \cap [a,b] = \cup_{j=1}^{\infty} [J_j \cap (u^*,\infty) \cap [a,b]] \cup \cup_{k=1}^{m} \mathcal{T}_k, \quad \text{for some} \quad m. \tag{A.10}$$

For $u \in (u^*,\infty)$ we have that $\frac{d}{du}(a^-(u)) = 0$, and hence

$$\frac{d}{du}\left(H_2^{BKLP}(u,u^-)\right) = -\frac{2(a^+(u))'(a^-(u))^2(u-u^-)}{(a^+(u)+a^-(u))^3}[Q(u)-A(u)] - \frac{(a^-(u))^2(a^+(u)-H'(u))}{(a^+(u)+a^-(u))^2}.$$

As in Case 1, we fix j and consider this time the corresponding interval $J_j \cap (u^*,\infty)$. Since a^+ is a smooth non-decreasing function on (u^*,∞) and $Q(u) > A(u)$ on J_j, the first term on the RHS ≤ 0. Also $a^+(u) \ge H'(u)$ and hence the second term is also ≤ 0. This gives that $H_2^{BKLP}(u,u^-)$ is a non-increasing function of u on $J_j \cap (u^*,\infty)$ for every j.

When $u^- < u^* < u$, $a^+(u) = H'(u)$, $a^-(u) = -H'(u^-)$, and hence

$$\frac{d}{du}\left(H_1^{BKLP}(u,u^-)\right) = \frac{a^-(u)H'(u)}{(a^+(u)+a^-(u))^3}G(u,u^-), \tag{A.11}$$

where $G(u,u^-)$ is given by (2.20). Since $H'(u) \ge 0$ for $u > u^*$, conditions (2.20)–(2.21) ensure that the RHS in (A.11) is ≤ 0 for $u \in \mathcal{T}_k$. This shows that $H_1^{BKLP}(u,u^-)$ is a non-increasing function on each of the intervals $\mathcal{T}_k$ constituting $V_1 \cap [a,b]$ (if $V_1 \cap [a,b]$ consists of finite number of points, then $H_1^{BKLP} \equiv H_2^{BKLP}$ at these points).

Since $H_1^{BKLP}(u,u^-) = H_2^{BKLP}(u,u^-)$ on ∂J_j, all the above arguments and (A.6) prove that H^{BKLP} is non-increasing on (u^*,∞). This, together with the conclusion in Cases 1 and 2 and the continuity of $H_i^{BKLP}(u,u^-)$, $i=1,2$, give that H^{BKLP} is non-increasing on $[a,b]$.

Similarly, one proves that $H^{BKLP}(u^+,u)$ (when u^+ is fixed) is a non-decreasing function of the second argument u. Here, in the case corresponding to (A.11) in Case 3b above, we have

$$\frac{d}{du}\left(H_2^{BKLP}(u^+,u)\right) = \frac{a^+(u)H'(u)}{(a^+(u)+a^-(u))^3}G(u,u^+), \quad u < u^* < u^+.$$

Since $H'(u) \le 0$ for $u < u^*$, conditions (2.20)–(2.21) guarantee that the derivative is non-negative, and hence $H_2^{BKLP}(u^+,u)$ is a non-decreasing function of u on the finite union of closed intervals $S^+(u,u^+) \cap [a,b]$.

∎

Acknowledgment: The work of A. Kurganov was supported in part by the NSF Grant DMS-0196439. The work of D. Levy was supported in part by the NSF under Career Grant DMS-0133511. The work of G. Petrova was supported in part by the NSF Grant DMS-0296020.

References

[1] S. BRYSON AND D. LEVY, *Central schemes for multidimensional Hamilton-Jacobi equations*, NAS Technical Report NAS–01–014, 2001, SIAM J. Sci. Comput., to appear.

[2] S. BRYSON AND D. LEVY, *High-order central WENO schemes for 1D Hamilton-Jacobi equations*, Proc. Enumath 2001, Ischia, Italy, to appear.

[3] S. BRYSON AND D. LEVY, *High-order central WENO schemes for multi-dimensional Hamilton-Jacobi equations*, NAS Technical Report NAS–02–004, SIAM J. Numer. Anal., to appear.

[4] S. BRYSON AND D. LEVY, *High-order semi-discrete central-upwind schemes for multi-dimensional Hamilton-Jacobi equations*, NAS Technical Report NAS–02–006, J. Comput. Phys., to appear.

[5] M.G. CRANDALL, P.-L. LIONS, *Two approximations of solutions of Hamilton-Jacobi equations*, Math. Comp., **43**, (1984), pp.1–19.

[6] S. Gottlieb, C.-W. Shu and E. Tadmor, *Strong stability-preserving high order time discretization methods*, SIAM Review, 43 (2001), pp. 89–112.

[7] G.-S. JIANG AND D. PENG, *Weighted ENO schemes for Hamilton-Jacobi equations*, SIAM J. Sci. Comput., 21 (2000), pp. 2126–2143.

[8] G.-S. JIANG AND C.-W. SHU, *Efficient implementation of weighted ENO schemes*, J. Comput. Phys., 126 (1996), pp. 202–228.

[9] A. KURGANOV AND C.-T. LIN, *On the reduction of numerical dissipation in central-upwind schemes*, in preparation.

[10] A. KURGANOV, S. NOELLE AND G. PETROVA, *Semidiscrete central-upwind schemes for hyperbolic conservation laws and Hamilton-Jacobi equations*, SIAM J. Sci. Comput., 23 (2001), pp. 707–740.

[11] A. KURGANOV AND G. PETROVA, *Central schemes and contact discontinuities*, M2AN Math. Model. Numer. Anal., 34 (2000), pp. 1259–1275.

[12] A. KURGANOV AND E. TADMOR, *New high-resolution semi-discrete schemes for Hamilton-Jacobi equations*, J. Comput. Phys., 160 (2000), pp. 241–282.

[13] B. VAN LEER, *Towards the ultimate conservative difference scheme, V. A second order sequel to Godunov's method*, J. Comput. Phys., 32 (1979), pp. 101–136.

[14] C.-T. LIN AND E. TADMOR, *L^1-stability and error estimates for approximate Hamilton-Jacobi solutions*, Numer. Math., 87 (2001), pp. 701–735.

[15] C.-T. LIN AND E. TADMOR, *High-resolution non-oscillatory central schemes for Hamilton-Jacobi Equations*, SIAM J. Sci. Comput., 21 (2000), pp. 2163–2186.

[16] X.-D. LIU, S. OSHER AND T. CHAN, *Weighted essentially non-oscillatory schemes*, J. Comput. Phys., 115 (1994), pp. 200–212.

[17] P.E. SOUGANIDIS, *Approximation schemes for viscosity solutions of Hamilton-Jacobi equations*, J. Differential Equations, 59 (1985), pp. 1–43.

[18] P.K. SWEBY, *High resolution schemes using flux limiters for hyperbolic conservation laws*, SIAM J. Numer. Anal., 21 (1984), pp. 995–1011.